FIELDSTON SCIENCE BULLETIN
ISSUE 1 // VOLUME 5 // JUNE 2025

THE SPRING AND SUMMER DOUBLE ISSUE

EDITOR IN CHEIF ..... CRISTINA ELLIS

FACULTY ADVISOR..... MS. BEATON

CONTENT ADVISOR.....FRANCESCA MASTER

SCAN THE QR CODE FOR THE ARTICLE AND IMAGE SOURCES LIST!

HOW DO BEACHES FORM?

Cristina Ellis

Summer has long been synonymous with visits to the seaside. All season long, people flock to the coast to soak up the sun and frolic in the crashing waves, but few know how these unique landforms come to be.

Beaches are narrow strips of sloping land along the edge of lakes, rivers, or oceans. They are covered by various materials, including sand, rocks, and even shells. Beaches are formed by erosion caused by the water that borders them. Over time, the water ears away at the land and nearby rocks, forming sand.

The changing tides deposit more sand and ocean sediment on the shore, creating the beaches we so enjoy. Constructive waves build up beaches the most because they have a strong swash (the thin sheet of water that washes up after a wave breaks) and a weak backwash. Commonly, sandier beaches are found where the water is shallow, as waves have less energy.

Waves and tides aren't the only things that affect these coastal landforms; changing weather patterns due to seasonal changes also affect beaches. During winter,

storm winds can pick up sand and carry it through the air. This action causes beaches to be eroded and can form sandbars. During the calmer summer months, waves retrieve sediment from the sandbars and carry it back to the beach. Because of this, beaches tend to be narrower and have steeper drop-offs in the winter, and tend to be wider and have a gentler slope in the summer.

Winds also create another unique feature of beaches: sand dunes. These dunes form when the wind blows sand into a sheltered area behind a large obstacle; over time, the sand accumulates into a small mound. Every dune has a windward side (the side on which the wind blows and pushes the sand upwards) and a slipface. Usually, the slipface is smoother than the textured windward side. These dunes have many benefits. In addition to providing a natural barrier against erosion, they also serve as a protective barrier from storm surges, saving coastal communities from flooding.

Beaches hold a special place in many people's hearts as an enduring symbol of summer. This year, when you find yourself wandering down the shore, be sure to stop for a minute and appreciate the natural splendor around you. Beaches are the product of years of work by Mother Nature and are not to be taken for granted.

HOW DOES CHLORINE CLEAN POOLS?

Francesca Master

When you think of summer activities, one of the first things that will come to mind might be going to the pool on a sunny day! In most swimming pools, there is something called chlorine, which kills bacteria that are dangerous to humans. But how does chlorine clean these pools and ensure a safe and clean swimming environment for all?

Chlorine causes a chemical reaction that breaks down hypochlorous acid (HOCI) and hypochlorite ion (OCI-). This reaction attacks the lipids in cell walls, as well as the cell's internal structures and enzymes, making them oxidized and harmless. Hypochlorous acid can do this in several seconds, whereas the hypochlorite ion can take 30 minutes.

The pool's pH plays a significant role in the effectiveness of chlorine. An ideal pH range to ensure effective pool cleaning is between 7 and 8. If the pH is too high, then it will take far longer to clean the pool. Once HOCI and OCI- finish cleaning the pool, they will combine with another chemical (for example, ammonia) or get broken down into single atoms. Sunlight speeds up the breakdown process. To ensure that the

pools stay clean, chlorine must be readded as the chlorine already in the pool is broken down.

Chlorine can have some adverse effects on swimmers. Many people find the smell of chlorine overwhelming or even sickening. Chlorine can also irritate one's skin and make them feel itchy, The hypochlorite ion can also cause fabrics to fade if they are not washed.

Thanks to chlorine, you won't have to worry about the cleanliness of your swimming pool this summer. While it may have some adverse effects, the safety it provides to swimmers is invaluable.

THE EFFECT OF CLIMATE CHANGE ON SPRINGTIME

Hannah Saez-Zadoff (with help from Cristina Ellis)

If we had no winter, the spring would not be so pleasant. This popular saying by Anne Bradstreet encompasses the feelings of when spring finally blooms after a long, hard winter. While it may feel like we are in an eternal cycle of seasons, going from warm highs to frigid lows, things are actually changing.

Across the globe, climate change has affected the seasons in many ways, one of the most prominent changes being higher temperatures year-round. As climate change brings warmer winters, America's spring growing season lasts longer. In fact, the season's length has grown by over two weeks in the past century. These warmer temperatures occurring earlier have affected farms all across America.

The frost-free season, defined as the period between the final occurrence of 32 ℉ in the spring and the first occurrence of 32℉ in the fall, determines the length of the growing season. In the contiguous 48 states, as well as Alaska, the frost-free season has grown, causing "drier conditions and higher temperatures." This will affect plant growth and may lead to farmers needing to experiment with alternate methods of crop growing to accommodate the changing environment.

But what will happen if climate change is allowed to continue unchecked? Among the consequences of this new trend are: the earlier arrival of allergy season, likely higher consistency of droughts in the US, less water accessible from mountaintops, more pest issues in agriculture, and loss of pollinators like bees and butterflies.

One example of an annual tradition put at risk by changing seasons is the famous Washington D.C. cherry blossoms. The pink flowers are blooming earlier in the year, altering the time the annual festival begins and potentially harming the city's tourism. DC's beautiful cherry trees are also at risk of being weakened by the nearby Tidal Basin's flooding, an effect of rising sea levels.

Spring is cherished by many as a season of renewal, marking nature's rebirth after the harsh winter months. But if climate change continues unchecked and alters the character of the season, will it still hold the same place in our hearts?

FSB SUN FACTS

FSB Staff

In every issue of the FSB, we like to publish a series of scientific fun facts so readers can learn a little bit about a wide array of topics. For our summer issue, we decided to publish a series of Sun facts as well as fun facts!

1. How hot is the sun?

The hottest part of the Sun is its core, where temperatures top 27 million °F (15 million °C). The photosphere, the surface of the sun, is cooler, only 10,000 °F (5,500 °C). The Sun's outer atmosphere, the corona, gets hotter the farther it stretches from the surface and reaches up to 3.5 million °F (2 million °C).

While the sun is the largest object in our solar system with a diameter of 865,000 miles (1.4 million kilometers), it's only an average star in terms of size. Other stars are larger (stars up to 100 times larger have been found) and hotter.

2. What causes a sunburn?

When skin is subjected to too much ultraviolet (UV) light, the skin cells are damaged. If the damage is beyond repair, the cells die and blood vessels dilate to increase blood flow and bring immune cells to the damaged skin. This causes the redness, swelling and inflammation known as sunburn. Sunburn can be caused by UV radiation from

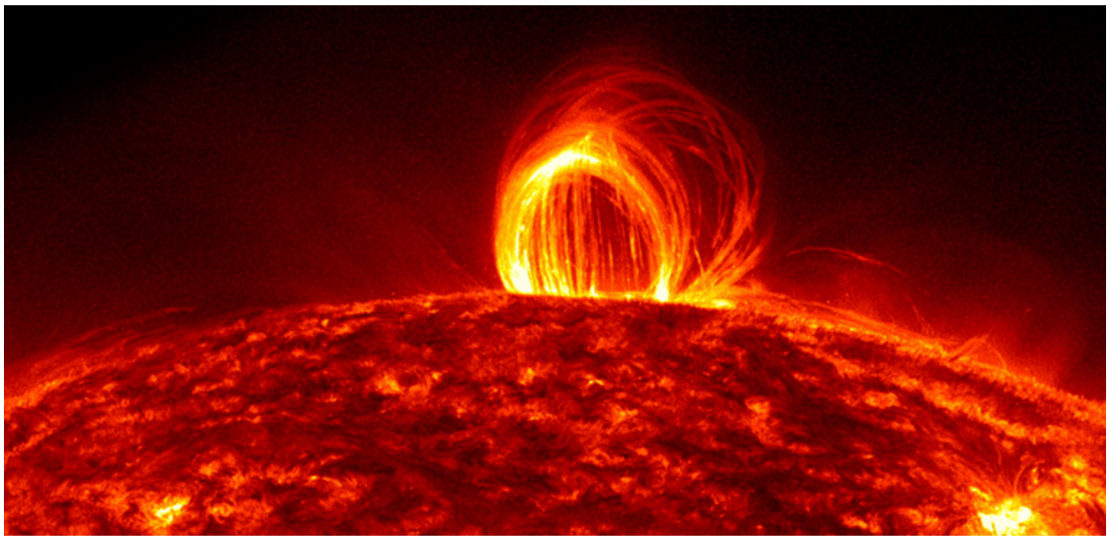

the sun or artificial sources, such as tanning beds.

Sunburns are categorized according to how deep the damage is in the layers of the skin. A first-degree sunburn is one in which there is damage to the skin's outer layer (epidermis). It will usually heal by itself in about a week. A second-degree sunburn is one in which the middle section of the skin (dermis) has been damaged. Blisters will develop and it may take weeks to heal. A third-degree sunburn is very rare. It severely damages all layers of the skin, including the fat layer beneath the skin. Most third-degree burns result from fires or chemical burns rather than sun exposure.

3. How does sunscreen protect the skin?

There are two types of sunscreen: organic sunscreens, also known as chemical sunscreens, and inorganic sunscreens, also known as physical sunscreens. Organic sunscreens are absorbed by the skin and protect the skin by absorbing UV radiation and transforming the energy into heat, which disperses from the skin. They typically include oxybenzone, avobenzone or octinoxate. These sunscreens are often designed to protect against both UVA and UVB radiation.

Inorganic sunscreen sits on top of the skin's surface and acts as a physical barrier that reflects and scatters UV radiation. They contain mineral compounds such as zinc oxide and titanium oxide.

A broad-spectrum sunscreen contains compounds that absorb and/or reflect both Ultraviolet A (UVA rays) and Ultraviolet B (UVB) rays. UVB is the principal cause of sunburn, but both UVA and UVB increase the risk of skin cancer. Many sunscreens combine organic and inorganic compounds to provide broad-spectrum protection.

4. How do sunglasses protect the eyes?

Sunglasses protect the eyes against harmful ultraviolet rays that can damage the cornea and retina. They also protect the eyes from intense light, which causes squinting and can damage the retina. Polarized sunglass lenses eliminate glare, and depending upon the type of lenses used, sunglasses can also block or enhance frequencies of light that blur vision or stimulate the body to go to sleep or stay awake.

5. What is Manhattanhenge and why does it happen?

Mahnattanhenge occurs when the alignment of the sun with Manhattan's street grid creates a radiant glow that simultaneously illuminates the north and south sides of every cross street. The sun only rises/sets due east/due west twice a year, on the Spring Equinox and the Autumn Equinox. Every other day, it rises and sets at other points on the horizon.

Manhattanhenge occurs on days when the sunrise or sunset aligns with Manhattan's street grid, which is rotated 29 degrees from true east-west. The sunset alignment occurs around May 28th and July 13th, and the sunrise alignments occur around December 5th and January 8th.

In addition to the rectilinear street grid, other unique features of Manhattan make Manhattanhenge possible – the clear view to the horizon across the Hudson River and the tall buildings that line the streets and frame the setting sun.

FSB FUN FACTS (SYMBOLS OF SUMMER)

FSB Staff

1. What is the science behind fireworks?

The impressive fireworks displays we enjoy on July 4th are the result of a series of chemical reactions. The shell is the main part of the firework. The bottom of the shell contains the lift charge, which is made of black powder. Black powder was developed by Chinese alchemists over 1,000 years ago and is composed of potassium nitrate (75%), charcoal (15%), and sulfur (10%). The shell also contains small pellets known as stars, which produce the colors, sounds, and other effects we see in the night sky.

When the firework fuse is lit and the black powder is ignited, it produces hot gases and energy that force the shell out of the tube it is sitting in (the mortar) into the sky. A second fuse ignites when the firework reaches a certain height and activates the burst charge, which ignites the stars in the shell. The result is the dazzling array of colors, sounds, and other effects we so enjoy.

The size and content of the stars in the fireworks determine the effects we see. Stars that contain metal salts produce brilliant colors. For example, strontium produces red, barium produces green, and copper produces blue.

Other chemical compounds are responsible for light effects such as strobing, sparkling and flashing. For example, adding aluminum produces white sparks, iron produces gold sparks and various types of charcoal can produce red and orange sparks.

Sound effects are also the result of chemical reactions. For example, adding bismuth creates a crackling or popping effect. Other chemical compounds can be packed tightly into a tube to create a slow burn, which results in a slow release of gas that creates a whistling sound.

2. What gives popsicles their unique texture?

When water freezes, crystals develop as the molecules arrange themselves in a hexagonal lattice. The freezers that popsicle manufacturers use are much colder than the freezers that we have at home, which enables them to cool the liquid faster, giving the molecules less time to form large ice crystals. Additionally, additives that accelerate the rate at which the liquid freezes or increase the viscosity of the liquid may be added, further impeding the growth of large ice crystals.

Commercial popsicle manufacturers add stabilizing ingredients to prevent the ingredients in the popsicle from separating during freezing, which can happen if some of the ingredients have a lower freezing point than water. This keeps the syrup, flavoring, and other ingredients from separating from the ice as it forms, and they act as a semi-frozen lubricant between the ice crystals, producing a popsicle with a slushy consistency.

3. What is the science behind barbecue's unique flavor profile?

Cooking over an open flame subjects food to very high temperatures ranging from 500 to 700 degrees Fahrenheit. If you are grilling a piece of meat, this causes the water near the surface to boil off, and then the amino acids and sugars in the meat undergo a chemical reaction known as the Milliard Reaction. This produces melanoidins, a brown pigment that browns the meat, and a mixture of molecules contributing to the flavor profile. These include furanone (sweet, caramel-like flavor), pyrazine, and thiophene (roasted flavor).

A similar process occurs when you barbecue vegetables. The high temperature evaporates the water in the vegetables, which prevents them from becoming soggy, and it promotes a process known as caramelization. This transforms carbohydrates and sugars into compounds including diacetyl (butter-like flavor), esters and lactones (sweet, almost rum-like flavor), furans (nutty flavor), and maltol (toasty flavor). Caramelization also impacts the flavor of barbecue sauce, which contains sugar.

Charring and smoky flavors are hallmarks of barbecued food. Charring occurs when prolonged exposure to heat causes non-carbon atoms in the food to break down,

leaving behind the crispy, black carbon. The smoky flavors are the result of the food absorbing smoke produced by the wood or charcoal fueling the grill. This smoke comprises gases, water vapor, and small solid particles from the fuel. Burning wood produces molecules, including syringol and guaiacol, that are responsible for the quintessential smoky flavor we associate with barbecue.

4. How do fireflies light up?

Fireflies emit light due to a biochemical reaction known as bioluminescence, which occurs in the insect's light organ. Light is produced when oxygen combines with calcium, adenosine triphosphate, and luciferin in the presence of luciferase, a bioluminescent enzyme. A firefly controls the beginning and end of the chemical reaction, and thus the start and stop of its light emission, by adding oxygen to the other chemicals needed to produce light. They transport oxygen from outside of their bodies to the interior cells through a complex series of tubes known as tracheoles. Fireflies produce cold light, not the hot light produced by lightbulbs.

Fireflies light up for various reasons, including attracting mates and warding off predators. Many fireflies have flash patterns unique to their species.

[89ZR]ZR-DFO-SIBROTUZUMAB AS AN ACTIVE TARGET FOR THE FIBROBLAST ACTIVATION PROTEIN (FAP)

Sophia Thompson

Abstract:
Radiopharmaceuticals represent a cutting-edge cancer diagnosis and treatment approach by combining radioactive isotopes with active molecules for targeted delivery. This study examines the potential of active targeting with the humanized monoclonal antibody sibrotuzumab, which binds to the fibroblast activation protein FAP, a protein overexpressed by cancer-associated fibroblasts (CAFs) in the tumor microenvironment. Utilizing U-87, glioblastoma cells that endogenously express FAP, the binding affinity, and internalization of [89Zr]Zr-DFO-sibrotuzumab were examined through antibody internalization assay at 4 and 37 degrees Celsius. Before the execution of the assay, successful bioconjugation of the antibody with the chelator DFO was confirmed by conducting an iTLC analysis and radiolabeling with zirconium-89. The results of this assay demonstrated consistent membrane binding of over 50% at both temperatures. This indicates a strong affinity for sibrotuzumab for FAP. The internalization rates for FAP varied with temperature and were relatively; however, because the primary aim of this study was to validate FAP as a viable target for future radiopharmaceutical development, and the internalization rates do not affect its viability as a target, it is just an extra statistic. These findings support further investigation into sibrotuzumab-FAP targeting in more complex tumor models. This can include in vivo biodistribution studies and tumor microenvironment simulations.

Introduction:
Radiopharmaceuticals are vital to the healthcare industry. They serve as an intersection between medicine, chemistry, and radioactivity, a new field that is evolving every day.[1] Nuclear medicine procedures are instrumental in imaging and targeting malignancies; millions are performed yearly. Designing and engineering radiopharmaceuticals is a complicated process that requires multiple factors to align for the drug to work. Choosing the appropriate nuclide is critical as each has a specific half-life and decay type that must be worked with and around to create a successful radiopharmaceutical. These factors impact the utility and localization of radiopharmaceutical products as well. Molecular stability, ease, and production cost are also critical when designing radiopharmaceuticals, as the field is costly and often challenging to produce results quickly.[2]

The combination of radioisotopes and medicine is an integral part of modern medicine. It combines innovation and science to transform disease diagnosis, treatment, and understanding. Radioisotopes act as invisible markers, allowing medicines to go beyond what most understand as traditional medicine. They are much more customizable to each patient, assisting in making treatments more effective and lowering side effects.

In the quest for the best radiopharmaceutical cancer treatments, scientists explore the best combinations of the pieces explained below. There are two main types of radiopharmaceuticals: passive targeting and active targeting. This paper will focus on active targeting, which this project focuses on as its research into radiopharmaceutical anticancer treatments. Active targeting is an approach in which a ligand, usually an antibody, small molecule, or peptide, is attached to a radioactive molecule, a radioisotope. This targeting method is specifically designed to deliver radiation to cancer cells or the stroma of cancer cells that express specific receptors. This method minimizes the toxicity of radiopharmaceuticals and enhances their therapeutic effectiveness.[3] There have been several successful radiopharmaceuticals that use active targeting, including Lutetium-177 (Lutathera), which was approved by the FDA in 2018, targeting the somatostatin receptor overexpressed in gastroenteropancreatic neuroendocrine tumors.[4] Another example is Technetium-99m, mainly used in diagnostic imaging.[5]

Compared to older treatment methods, modern radiopharmaceuticals specifically deliver radiation therapy. Unlike external radiation, which can often cause collateral damage, as normal tissue has to be hit to get to cancer, radiopharmaceuticals can provide radiation therapy directly and specifically only to cancer cells, potentially reducing the short and long-term side effects of radiation treatment.[6]

Radiopharmaceuticals are drugs that consist of a radioactive form of chemical elements known as radioisotopes.[7]

Radiopharmaceuticals can be given orally, by injection, or intravenously, and their distribution can be monitored by screening with PET/CT, SPECT, or Gamma cameras.

Radiopharmaceuticals must target a specific body area because of their highly toxic nature.

Radiopharmaceuticals consist of four pieces: the radioactive isotope of a metal, a chelator, a linker, and a targeting molecule. While the purpose of a drug can determine the choice of radiometal, our lab was interested in exploring a specific antibody. Therefore, the radiometal came last, as it was first looked at to see which chelator works with the antibody and which radiometal can work with that chelator. Radioligands can emit EC (electron capture), β + decay, β- decay, and ∝ decay. β+ decay and β- decay are involved in positron emission tomography. When an annihilation reaction occurs, gamma waves shoot 180 degrees, creating an image shows where the radiopharmaceutical is in the body.

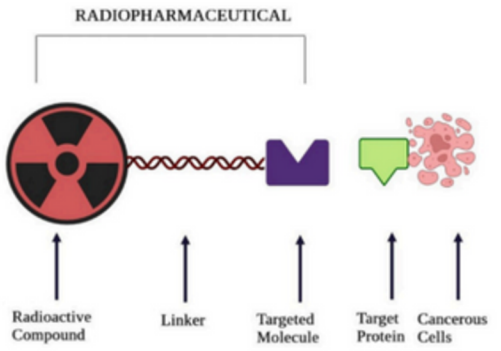

A bifunctional chelating agent (BFC) must bind the radiopharmaceutical to the targeting molecule to bind the two together. The BFC attaches to the radioisotope and can also attach to the linker, functioning as both a transitional piece and a protector of the radioisotope. This ensures that the radioisotope is not released into the body while in transit to its targeted location.[8] The BFC protects the radioligand from competing bioligands and attaches it to the drug's targeting agent. A linker connects the BFC radiometal piece to the targeting molecule. It can be optimized to improve tumor uptake, distribution, and pharmacokinetics.[9]

Targeting molecules can vary dramatically depending on the radiopharmaceutical. Generally, targeting molecules are small-molecule inhibitors or antibodies pertaining to radiopharmaceuticals. These targeting molecules aim at specific genes, proteins, and other molecules involved with cancer cells' growth, spread, and survival. The targeting molecule binds to its target, and therefore, the rest of the radiopharmaceutical is attached, and the radioactive compound can decay.

The Jason Lewis lab focuses on developing radiopharmaceuticals for targeted diagnosis and treatment of cancer. In my project, we looked at the antibody sibrotuzmab, a humanized monoclonal antibody intended for cancer treatment. It targets the fibroblast activation protein (FAP), a protein expressed by Cancer-Associated Fibroblasts (CAFs), a group of activated fibroblasts that secrete a variety of factors regarding tumor regulation. The goal of this project was to look at the internalization and the binding of the antibody sibrotuzmab to FAP and to determine its affinity to FAP as a target; see Appendix 2 for more details.

Methods:

We used bioconjugation and cell culturing to develop the cells necessary to perform the antibody internalization assay. The cell line U-87, a glioblastoma cell line, was used as a model for this experiment, as U-87 endogenously expresses the FAP target. U-87 cell line was grown in media, MEM+NEAA+10% FCS, and was grown in flasks. The steps were as follows.

1. We performed a bioconjugation to bind the Sibrotuzumab antibody with DFO in DMSO. This was completed twice, with a new batch of DFO used the second time. The DFO dissolved successfully in DMSO, allowing for the correct ratio of DFO in DMSO, as stated in the procedure (Appendix One).

2. U87 cells were cultured for five weeks to perform an antibody internalization assay. The cells were grown in flasks containing media. Cells were grown on the flask's long, flat, horizontal side. The media was changed

every 2-4 days based on the media's color and then the cells' concentration in the flask. The higher the concentration, the more often the media needed to be changed and the higher the likelihood that the cells needed to be split into more flasks to prevent their death. When splitting cells, trypsin was used to remove the cells from the wall of the flask, and for every unit of trypsin, an equal amount or more of media was used to ensure that the trypsin did not kill the cells. After this cell mixture was created, it was centrifuged to isolate the cells for their transfer into new flasks. See Appendix Two for a more specific procedure.

3. Once the cells were grown and the bioconjugation completed, a test radiolabeling was performed to ensure its success. An iTLC test was performed to double-check that the zirconium stuck onto the bioconjugation instead of traveling up the strip. This was successful; therefore, this bioconjugated piece could be used for the antibody internalization assay. Radiolabeling is a very time-sensitive procedure. It was important to consistently mark the time and the number of millicuries in the amount of ml Zr-89 at every step of the procedure.

4. As stated in the procedure above, an antibody internalization assay was completed utilizing bioconjugation. 3µl of radioligand was placed in each Eppendorf tube, which held 200µl of U87 cells. Half of the cells were incubated at 37C, and the other half at 4C, to test for the effect of temperature on the internalization assay. This was done for 90 minutes, and the cells were tapped/shaken up and down every 15 minutes. Once incubated, each tube was centrifuged to remove the supernatant, then wash 1, wash 2, glycine 1, glycine 3, and finally hydroxide. These tubes were promptly placed on the gamma counter to determine the amount of radioactivity in each before all radioactivity was gone.

Experimental Results:

This experiment aimed to determine the percentage of [89Zr]Zr-DFO-sibrotuzumab bound to the membrane of the U-87 cell and then the

amount that was internalized into the cell. This required testing iTLC to ensure that the iTLC machine was working correctly. Then, an iTLC test was performed on the radiolabeled bioconjugated piece to ensure that it was properly radiolabeled before using [89Zr]Zr-DFO-sibrotuzumab to conduct the antibody internalization assay to see how much of the radioligand was internalized and how much bound to the membrane. Additionally, temperature was considered a variable, with 4 degrees and 37 degrees Celsius being the two different temperatures at which this experiment was conducted.

Figure 1: Control iTLC Test

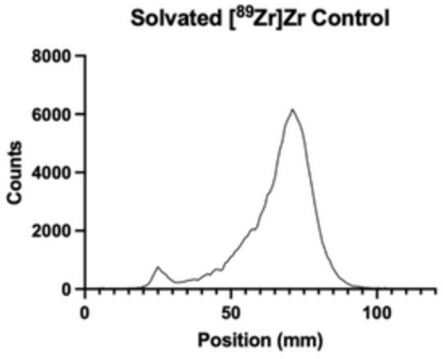

Figure 1 presents a control iTLC test of solvated [89Zr]Zr, demonstrating an incorrect iTLC and what it looks like when the [89Zr]Zr is not correctly radiolabeled to the bioconjugation piece. The initial small spike is where the solution was pipetted onto the 100 mm strip, between approximately 20mm and 30mm up the strip

Figure 2: iTLC Test of the Bioconjugation with [89Zr]Zr-DFO-sibrotuzumab

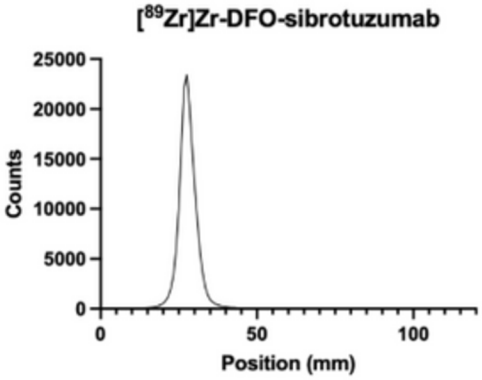

Figure 2 presents a successful radiolabeling of [89Zr]Zr with sibrotuzumab. The radiolabeled solution was placed approximately 25-35mm up the strip. The solution stayed there, and the [89Zr]Zr did not travel up the sheet, indicating that the [89Zr]Zr bonded correctly to the bioconjugated piece.

Figure 3: Average Percent of [89Zr]Zr-DFO-sibrotuzumab Membrane-Bound and Internalized at 37 degrees and 4 degrees Celcius

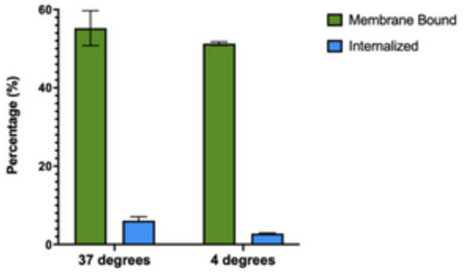

Figure 3 presents the average percentage of [89Zr]Zr-DFO-sibrotuzumab that is membrane-bound and the average percentage of [89Zr]Zr-DFO-sibrotuzumab that is internalized at 37 degrees and 4 degrees.

Table 1: Antibody Internalization Assay at 37 Degrees

Tube	Membrane-Bound	Internalized
C1	57.4	6.9
C2	50.1	5
C3	58.2	6.4
Average	55.2	6.1

Table 1 presents the data of the antibody internalization assay at 37 degrees Celsius. This experiment was repeated three times, and the average of those repetitions is indicated on the bottom of this table.

Table 2: Antibody Internalization Assay at 4 Degrees

Tube	Membrane-Bound	Internalized
C1	51.0	2.9
C2	51.6	2.7
Average	51.3	2.8

Table 2 presents the data of the antibody internalization assay at 4 degrees Celsius. This experiment was repeated three times, and the average of those repetitions is indicated at the bottom of this table.

Discussion:

This project aimed to look at the internalization and the binding of the antibody sibrotuzmab to FAP and to determine its affinity to FAP as a target. The affinity to the FAP was found to be quite high, and the data can be used to continue this experiment and utilize the FAP as a target when creating radiopharmaceuticals. Before this experiment could be conducted, it was essential to ensure that the bioconjugation had been successful. The bioconjugation links the chelator with the antibody sibrotuzmab, the targeter of the FAP. If these molecules are not linked properly, the radioligand (the chelator

and radioactive material) could detach from the radiopharmaceutical, potentially harming the organism it is in. Free-floating radioligands can go into the bloodstream and the bones and be potentially lethal. The next step of an experiment like this is a biodistribution study, in which small animals are injected with radiopharmaceuticals and assayed for radiation at different locations throughout the body and in the tumor. An intermediate step is to radiolabel a solvated control and the bioconjugated piece and to test its success with an iTLC test strip. In our experiment, the control was shown in Figure 1, and the successful radiolabeling of DFO-sibrotuzumab with [89Zr]Zr is shown in Figure 2.

We performed the test by radiolabeling a solvated [89Zr]Zr control to demonstrate what a successful bioconjugation should not look like, and then performing an actual radiolabeling of [89Zr]Zr-DFO-sibrotuzumab. By comparing the two graphs, Figure 1 and Figure 2, it is clear that the radiolabeling of the control is not successful, as expected. This is clear by the shape of the graph; between 20-30mm up the iTLC strip, there is a small peak where the main peak should be, and there is a large peak further up the iTLC strip, meaning that the radioligand has been carried up, and was not successfully attached to the bioconjugated molecule. Figure 2 shows the graph's peak at 20-30 mm, meaning that it was successfully bioconjugated because the radioligand was not carried up the strip.

The second part of this experiment could be conducted with a successfully bioconjugated ligand. An antibody internalization assay could be performed to examine the amount of sibrotuzumab that would bind to the outside of the cell and the amount that would be internalized into the cell. The measurement of the amount internalized was not necessary to conclude the results of this experiment, the goal of which was just to test the FAP as a target, which is on the outside of the cell. However, because of the model cell used, U-87, FAP as a target is also in the

inside of the cell. The assay broke down each cell layer by doing many different washes, including a media wash, two glycine buffer washes, and two hydroxide buffer washes. Each wash allowed for different breakdowns of the cell so that the gamma counter could look at the amount of the radioligand not attached (the media wash), the amount of radioligand attached to the membrane (the glycine buffer washes), and the amount of radioligand internalized into the cell (the hydroxide washes). Figure 3 shows the average percent internalized and the average percent membrane bound at 37 degrees and 4 degrees. Both temperatures had an average percent membrane-bound above 50%, which is promising. The target, FAP, is considered a type of CAF (cancer-associated fibroblast), which is the most prevalent TME (tumor micro-environment) cell; having numbers above 50% means that sibrotuzumab is a good targeting molecule for attaching onto the FAP, and is the reason why the amount of sibrotuzumab internalized is not important.

A limitation of this test of FAP as a target with sibrotuzumab is that this model does not test FAP as a target in a CAF in a TME. Without testing FAP as a target in the appropriate environment, one cannot know for sure that the sibrotuzumab would successfully bind to the FAP. However, despite this limitation, this study does show that sibrotuzumab has a strong affinity for FAP as a target.

Future experiments could include creating a TME with CAFs to test FAP as a target in its actual environment, as stated above. Another continuation of this study would be to do a bio-distribution at different time intervals to test how long sibrotuzumab stays bound at its target, the FAP, on the surfaces of the U-87 tumor cells. Our experiments show that sibrotuzumab is at least promising as an anticancer agent, and we hope that future in-vivo experiments will validate this.

Scan For Appendix and Bibliography

THE EFFECT OF GAMMA-SECRETASE INHIBITORS ON THE NOTCH AND WNT/B-CATENIN PATHWAY IN UTERINE LEIOMYOSARCOMA

Gabrielle Santemma

Abstract:
Uterine Leiomyosarcoma (uLMS) is a rare, aggressive cancer with poor response to standard chemotherapies. The NOTCH pathway is an evolutionarily conserved signaling pathway with oncogenic properties; when acting non-canonically/pathologically, it frequently activates the complementary Wnt/B-Catenin pathway. Both pathways rely on gamma-secretase to function properly. This prompted us to investigate the efficacy of gamma-secretase inhibitors in downregulating those downstream effectors involved in the development and metastasis of uLMS. Two uLMS cell lines, SK-LMS-1 (vulvar metastasis) and SK-UT-1B (uterine primary), were grown in media supplemented with 10% fetal bovine serum. Each cell line was then treated with MK-0752 or a combination therapy of MK-0752, gemcitabine, and docetaxel (MGD), and the expression of select genes (HES1 for NOTCH and C-Myc and Cyclin-D1 for Wnt/B-Catenin) was measured. Treatment efficacy was assessed using qPCR and Western Blots. qPCR results revealed a significant HES1 downregulation in SK-LMS-1 cells and a slighter one in SK-UT-1B cells when treated with MK-0752, indicating effective NOTCH pathway inhibition. MK-0752 and MGD treatments had varying efficacy in regulating C-Myc and Cyclin-D1 expression, indicating some (inconsistent) impact on the Wnt/B-Catenin pathway. Overall, SK-LMS-1 cells responded more favorably to treatments than did SK-UT-1B cells. Western blot analysis identified the present proteins as C-Myc and verified that MK-0752-treated samples had lower protein intensity and saturation than their control counterparts. This study demonstrates the potential of gamma-secretase inhibitors in targeting key signaling pathways of uLMS, thus suggesting their viability as an effective treatment for the malignancy.

Introduction:
Uterine Leiomyosarcoma (uLMS) is a rare and aggressive malignancy arising from smooth uterine muscle cells. It accounts for 65% of uterine sarcomas (Abedin et al., 2022). Current treatments of the disease depend on staging: early stages are generally treated via surgery, while advanced stages may use surgery in combination with common chemotherapies (including doxorubicin, gemcitabine, and docetaxel) (Abedin et al., 2022). Despite such treatment options, the five-year survival rate of patients with early-stage uLMS is under 50% and dro1ps to just 15% in advanced-stage patients (Abedin et al., 2022). uLMS also has exceptionally high recurrence rates, ranging, on

average, from 50-70% (Abedin et al., 2024). The disease remains a challenge to diagnose and treat, as its symptoms (abnormal uterine bleeding, an enlarged uterus, and/or pelvic pressure) often mimic those of benign gynecological conditions (Abedin et al., 2022). Women's health issues are also historically underdiagnosed, making it all the more challenging for those affected by uLMS to receive a timely diagnosis. Further, standard chemotherapy treatments frequently come with debilitating side effects, making it difficult for patients to consume effective doses (Abedin et al., 2024). Even at effective doses, studies have found that chemotherapy treatments do not lower recurrence rates to a statistically significant degree (Abedin et al., 2022). Thus, there exists a need for improved treatment options.

One promising but largely unexplored therapeutic strategy hinges on inhibiting the NOTCH signaling pathway. The NOTCH pathway is an evolutionarily conserved signaling pathway that plays an oncogenic role in many cancers, including uLMS (Abedin et al., 2022). In the canonical pathway, a NOTCH ligand binds to a NOTCH receptor, triggering the release of Notch Intracellular Domain (NICD) via the action of gamma-secretase. The NICD translocates to the nucleus, where it forms a complex with DNA-binding transcription factors (like CSL/RBPjk) (Abedin et al., 2022). This ultimately results in the transcription of downstream effectors like HES1 (Abedin et al., 2022). Gamma secretase plays a critical role in the cleavage of the NOTCH receptor and consequently in the expression of downstream effectors. Thus, gamma-secretase inhibitors, such as DAPT and MK-0752, can be used to effectively block the NOTCH pathway (Abedin et al., 2022). The pathway can also act non-canonically. This will occur when a non-canonical NOTCH ligand binds to the receptor, thus triggering a signaling cascade independent of the usual transcription factors (Anderson, 2012). The non-canonical pathway is generally associated with pathological conditions. Such non-canonical activation can trigger several cellular responses; notably, it may

activate other signaling pathways, including the Wnt/β-Catenin pathway (Anderson, 2012).

The Wnt/β-Catenin pathway is involved in several aspects of leiomyoma genesis (Sabeh, 2021). Studies have shown that selective overexpression of constitutively activated β-catenin in uterine mesenchyme during embryonic development -- and in adults-- gave rise to leiomyosarcoma-like tumors in the uterus of female mice (Tanwar, 2009). In the pathway, an extracellular Wnt ligand binds to a cell membrane receptor. This results in the formation of a multimeric protein complex, which promotes the dephosphorylation of β-Catenin. β-Catenin is thus able to accumulate in the nucleus and bind transcription factors, ultimately resulting in an increased expression of downstream target genes (like Cyclin D1 and C-MYC) (Sabeh, 2021). An over-accumulation of β-Catenin will result in over-expression of downstream effectors; this is primarily associated with pathological conditions (namely cancers like uLMS). Gamma-secretase inhibitors can prevent over-accumulation of β-Catenin by blocking the cleavage of E-cadherin (Sabeh, 2021). Given the Wnt/B-catenin pathway's involvement in uLMS and its interactions with the NOTCH pathway, gamma-secretase inhibitors could effectively inhibit both pathways (Barat, 2017)

Considering the high recurrence rate, poor survival outcomes, and general inefficacy of existing uLMS treatments, it is evident that novel therapeutic techniques are necessary to combat the disease and improve patient outcomes. We aimed to determine whether directly targeting the NOTCH and Wnt/β-Catenin pathways with a gamma-secretase inhibitor might be an effective treatment plan. To test this hypothesis, uterine leiomyosarcoma cells were treated with the gamma-secretase inhibitor MK-0752 and a combination therapy of MK-0752, gemcitabine, and docetaxel (MGD), and the RNA and protein expression of their downstream effectors were measured.

Methods:

Cell treatment:

Two cell lines were cultured to investigate this aim: SK-LMS-1, a vulvar metastasis from uterine leiomyosarcoma, and SK-UT-1B, a primary uterine leiomyosarcoma cell line with epithelial-like morphology. One line represents one patient, and thus, using two lines allows greater accuracy in results. Both cell lines were grown in media supplemented with 10% fetal bovine serum. Then, SK-LMS-1 and SK-UT-1B cells were serum starved for 4 hours and treated with either DMSO control, 1C30 concentration of MK-0752 alone, or in combination with gemcitabine and docetaxel (MGD) for 72 hours. 72 hours was chosen as the treatment time since this time frame was utilized in the lab's most recent paper (Abedin et al., 2024). RNA extraction was then performed on the cells.

RNA extraction:

To begin RNA extraction, 1x107 lysed cells were added to a petri dish. 600 ul of Buffer RLT Plus was added to the dish, and its contents were homogenized using a pipette. The homogenized lysate was then added to a gDNA Eliminator spin column placed in a 2ml collection tube and was centrifuged for 30 seconds at 8000 rpm. The column was then discarded, and 600 ul of 70% ethanol was added to the flow-through (the cellular debris and proteins that pass through the matrix) and thoroughly mixed. Next, 700 ul of the sample was transferred to an RNeasy spin column and centrifuged at 8000 rpm; this time, the resulting flow-through was discarded. 700 ul of Buffer RW1 was then added (in a 2 ml tube) to the same spin column and centrifuged at 8000 rpm for 15 seconds. 500 ul Buffer RPE was added to the spin column and centrifuged under the same conditions (any resulting flow-through was again discarded). This was repeated once more. The RNeasy spin column was transferred to a new 1.5 ml collection tube, and 50 ul of RNeasy free water was added directly to the spin column membrane. It was then centrifuged for one minute at 8000 rpm to elute (release from the matrix) the RNA. Eluting the RNA allowed for its collection and storage to later make complementary DNA (cDNA).

cDNA:

To make cDNA, RNA

concentrations were determined using a nanodrop machine from MRF. Then, the amount of RNA needed for 1ug RNA concentration per 20ul of cDNA was calculated. To dilute the RNA, the calculated quantity of RNase-free H2O was pipetted into each tube. Next, 5x Buffer and the enzyme Reverse Transcriptase (RT) were added to the tube and mixed well. Lastly, the calculated RNA quantities were pipetted into their respective tubes. The samples were then vortexed in a centrifuge and run in the PCR machine for 40 minutes. The resulting cDNA was then used to perform a quantitative PCR (qPCR).

qPCR:

A qPCR was performed to determine the efficacy of each treatment (DMSO, MGD, MK-0752) in downregulating selected downstream target genes of the NOTCH and Wnt β-Catenin pathways. To begin, cDNA was diluted to ¼ (10ul of cDNA to every 30ul of H2O), so the total concentration per sample was 12.5 ng/ul. Next, a mastermix containing Qiagen SYBR, Forward and Reverse primers, and H2O was made. To determine the proper quantities of each component, a pre-set number (10ul for SYBR, 0.4ul for forward and reverse primers, and 7.2ul for H2O) was multiplied by the number of wells in the qPCR plate, plus four extra to increase the margin of error (ex; for a plate with 36 wells, each pre-set quantity would be multiplied by 40). cDNA was then thawed on ice and vortexed in the centrifuge for 30 seconds. 18ul of the reagent mastermix was then pipetted into each well of an empty qPCR plate. The mastermix was followed by 2ul of diluted cDNA per well. Next, the entire plate was securely sealed and spun in the centrifuge. The plate was then transferred to the qPCR machine, which ran for 2 hours. Samples were then removed from the machine and discarded. The machine produced a graph that plotted the number of PCR cycles vs. fluorescent signals (which correlates to the quantity of target RNA in each sample), which was used for subsequent calculations. These calculations allowed researchers to determine the fold change in gene expression for each treatment group/gene combination, thus

quantifying treatment efficacy.

Western Blot:

A Western Blot was performed to verify the presence of C-myc protein and its expression level, thus allowing researchers to confirm Wnt/β-catenin pathway activity and subsequent treatment efficacy. First, C-myc protein (which had been previously treated with DMSO control or MK-0752) was obtained from a protein concentration assay, and an SDS-PAGE gel electrophoresis was conducted. In preparation, 4X Laemmli buffer and lysate were added to 1.5ml microcentrifuge tubes in a 1:4 ratio (regardless of ratios, the volume must never exceed 50ul). Next, a precast gel was removed from its packaging and placed into the gel housing unit of an electrophoresis machine. Its central chamber was then filled with 1X running buffer until the gel was fully submerged. The gel's comb was removed and each well was filled with 7ul of the aforementioned mixture (the first well was filled with 7ul of ladder). The remaining running buffer was then poured onto the center of the gel. The machine was closed and ran at 150-200V for one hour. While the electrophoresis ran, a nitrocellulose membrane was cut to approximately the size of the gel. The membrane, as well as sponges and filter paper, were then soaked in transfer buffer. The gel was removed from the electrophoresis machine and placed onto the filter paper. The gel/filter paper were transferred to a gel cassette on top of a sponge. An additional sponge was stacked atop the gel/filter paper, and the cassette's lid was replaced. The cassette was then placed into the plate electrodes and transferred to the buffer tank. The tank was filled to the top with transfer buffer and placed into a cooler with ice. It then ran at 40V for two hours.

Next, the protein detection procedure was performed. To confirm the transfer of proteins, a Ponceau staining was conducted (the membrane was immersed for 5 minutes on a shaker and then washed with TBS-T 5x for 5 minutes). Once protein was identified, the membrane was blocked for 60 minutes in 5% non-milk TBS-T. Next,

it was placed into a 50ml conical tube and covered again with 5ml of TBS-T and an appropriate dilution of the primary antibody. The membrane was then incubated overnight at 4℃ on a shaker. The next morning, it was washed three times with TBS-T (each wash was five minutes long). It was then blotted for two hours with the secondary antibody in 5% milk with TBS-T and washed three additional times.

Lastly, a chemiluminescence image (pictured below) was acquired. First, chemiluminescence reagents were mixed (2 ml total in a 1:1 ratio) and poured over the membrane. It was then incubated for five minutes; excess reagent was removed with Kim wipes at the edge of the blot. Lastly, the membrane was placed between two plastic sheets, and present proteins/their expression levels were assessed using ChemiDoc software.

Results:

A) SK-LMS-1 Gene Fold Changes

Sample	HES1	C-MYC	Cyclin-D1
DMSO	1.02	1.02	1.03
MK-0752	0.16	0.70	0.62
	p <0.01	*p = 0.18*	*p <0.01*
DMSO	1.05	1.06	1.02
MGD Combination	0.70	0.76	0.84
	p=0.02	*p=0.04*	*p=0.13*

B) SK-UT-1B Gene Fold Changes

Sample	HES1	C-MYC	Cyclin-D1
DMSO	1.03	1.02	1.04
MK-0752	0.59	1.03	1.08
	p=0.04	*p=0.99*	*p=0.7*
DMSO	1.02	1.10	1.04
MGD Combination	0.52	1.26	1.08
	p<0.01	*p=0.79*	*p=0.79*

Table 1: qPCR analysis of SK-UT-1B and SK-LMS-1 cell lines treated with a DMSO control, MK-0752, or the combination therapy MGD. The fold changes in expression of downstream target genes HES1, C-Myc, and Cyclin D1 were assessed, with statistical significance determined by t-test ($p < 0.01$). Results indicate the differential effects of each treatment on gene expression. Sample size = 6, repetitions = 3.

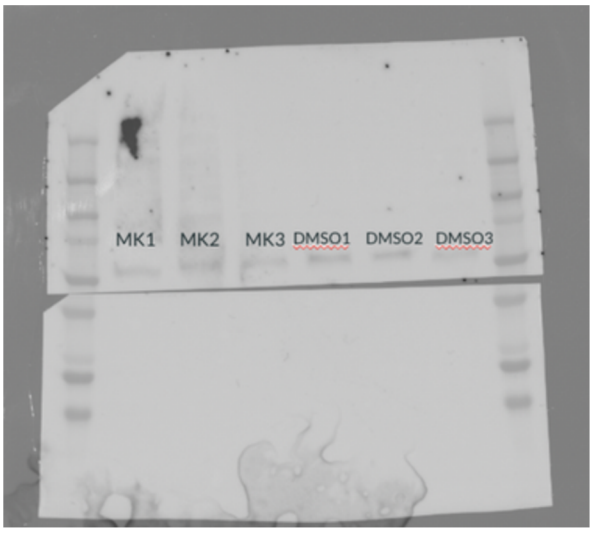

Figure 1: Western blot analysis of C-myc expression in MK-0752 treated samples vs DMSO controls. Band position corresponds to protein identity and band intensity to protein levels. The intensity and saturation of bands were determined by a western blot imaging machine. Sample size = 3, repetitions = 1.

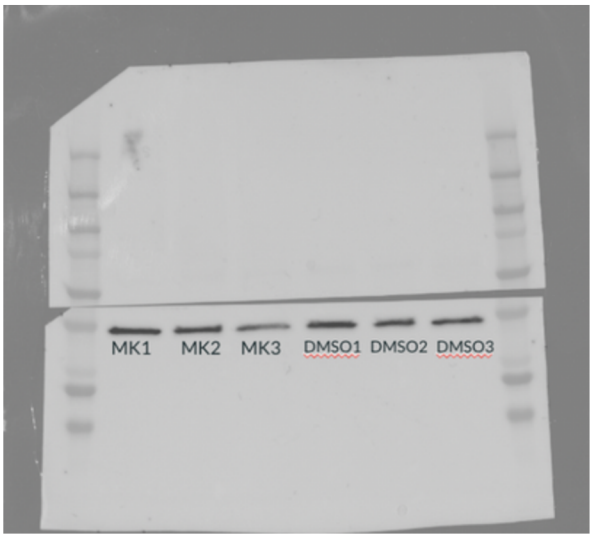

Figure 2: Western blot analysis of GAPDH (protein control) expression in MK-0752 treated samples vs DMSO controls. Band position corresponds to protein identity and band intensity to protein levels. The intensity and saturation of bands were determined by a western blot imaging machine. Sample size = 3, repetitions = 1.

Table 2: Average Intensity and Saturation of C-Myc and Control Proteins in Western Blot

	Average Intensity	Average Saturation (%)
GAPDH		
DMSO 1-3	41734.667	63.778
MK 1-3	41339.556	62.889
c-Myc		
DMSO 1-3	2707.111	4.333
MK 1-3	2554.667	3.889

Table 2: Average intensity (signal brightness from a protein band) and saturation percent (the degree to which pixels have reached their maximum possible intensity) of GAPDH control and c-Myc proteins treated with MK-0752 and DMSO control. Values were determined by a western blot imaging machine and averaged for comparative analysis across groups. Sample size = 3, repetitions = 1.

qPCR Results:

A qPCR analysis was performed on samples from SK-UT-1B and SK-LMS-1 cell lines treated with DMSO control, MK-0752, or the combination therapy MGD. The fold changes of three downstream target genes (HES1, C-Myc, and Cyclin D1) were measured, and statistical significance was calculated using a Mann-Whitney U test with an alpha level of $p < 0.01$. A fold change of 1 indicates no change in gene expression between experimental and control conditions, while a value <1 indicates a downregulation, and one >1 indicates an upregulation. In the SK-LMS-1 cell line, HES1 had a fold change of 0.16 when treated with MK-0752, 0.70 when treated with MGD, and 1.02 when treated with DMSO. While both MK-0752 and MGD treatments downregulated gene expression, only MK-0752 produced a statistically significant change, with a p-value <0.01. In the same cell line, MGD and MK-0752 treatments downregulated C-Myc expression (fold changes of 0.76 and 0.70, respectively), though not to a statistically significant degree (p-values of 0.04 and 0.18). However, MK-0752 treatment significantly downregulated Cyclin-D1 (fold change of 0.62 and p-value <0.01), indicating some effect on the Wnt/β-Catenin pathway. MGD treatment again downregulated Cyclin-D1 (fold change of 0.84), but not significantly (p-value of 0.13).

In the SK-UT-1B cell line, MGD treatment yielded significant HES1 downregulation (fold change of 0.52 and p-value <0.01). MK-0752, on the other hand, induced a slight but ultimately insignificant downregulation (fold change of 0.56 and a p-value of 0.04). Unlike in the SK-LMS-1 cell line, MGD and MK-0752 treatments slightly upregulated C-Myc and Cyclin-D1 expression. MGD produced a fold change of 1.26 in C-Myc and 1.08 in Cyclin-D1, while MK-0752 produced a change of 1.03 in C-Myc and 1.08 in Cyclin-D1. Thus, both MGD and MK-0752 treatments had a more pronounced effect on the downstream effectors of the NOTCH pathway than on those of the Wnt/β-Catenin pathway.

Western Blot Results:

A Western blot was performed to assess C-Myc expression in protein samples. Expression levels were determined by a Western blot imaging machine, which produced values of protein intensity (signal brightness from a protein band) and saturation percentage (the degree to which pixels have reached their maximum possible intensity). Lower protein intensity and saturation percentage indicate low protein expression. MK-0752 treated samples had lower protein intensity and saturation than their DMSO-treated counterparts. MK-0752-treated C-Myc samples exhibited an intensity that was 152.4 steps lower than that of DMSO-treated samples. Saturation was also reduced by 0.44%. This trend was observed in the GAPDH samples (a control "housekeeping" gene), which showed an average intensity decrease of 395.111 and a 0.89% reduction in saturation.

The western blot also functioned to confirm the identity of present proteins. It is known that C-Myc's molecular weight is 62 kilodaltons (kD). In Figure 1, the protein ladder aligns at the point corresponding to a weight of roughly 60 kD, identifying the protein as C-Myc.

Discussion:

qPCR

It was hypothesized that MK-0752 would downregulate gene expression in both SK-LMS-1 and SK-UT-1B cell line samples. Further, it was hypothesized that the combination therapy MGD would induce greater downregulation than MK-0752 alone. The results supported the former hypothesis, though not the latter one. The gamma-secretase inhibitor MK-0752 significantly downregulated HES1 in the SK-LMS-1 cell line; this was expected, as HES1 is a downstream target of the NOTCH pathway, which relies on gamma-secretase to function properly. MGD, however, did not significantly downregulate HES1, suggesting that the combination therapy may lack anticipated synergy. This data point is slightly at odds with previous findings, though it is worth noting that past experiments tested MK-0752 in combination with gemcitabine or

docetaxel independently of one another (Abedin et al., 2024). It is possible that antagonistic interactions between MK-0752-exposed gemcitabine and docetaxel are to blame for the lack of synergism. The same pattern was reflected in SK-LMS-1 Cyclin-D1 samples, further suggesting that the combination therapy lacks synergism, regardless of the pathway under observation (Cyclin-D1 being a downstream effector of the Wnt B-catenin pathway). A similar pattern was observed in SK-LMS-1 C-myc samples, though MK-0752 did not downregulate gene expression to a significant degree. Nonetheless, it produced a more substantial decrease than did MGD. Across all genes, the gene expression of samples treated with a DMSO control remained unchanged (as was expected).

MK-0752 downregulated HES1 in the SK-UT-1B cell line, though not significantly. This is reflected in previous papers, which found no significant decrease in SK-UT-1B NOTCH signaling when treated with MK-0752 (Abedin et al., 2022). MGD, however, produced a significant downregulation. This is the sole instance of MGD synergism, as the combination therapy produced a more significant downregulation than MK-0752 alone. C-myc and Cyclin-D1, however, responded differently to the treatments. MK-0752 slightly upregulated both C-myc and Cyclin-D1 in the SK-UT-1B cell line. MGD induced a severe upregulation in C-myc and a slighter one in Cyclin-D1. Such findings are consistent with previous studies, which demonstrated that SK-UT-1B cells exhibit lower sensitivity to gamma-secretase inhibitors than SK-LMS-1 cells; this difference in sensitivity may lead to varied gene expression responses (Abedin et al., 2024). Both upregulated genes (Cyclin D1 and C-myc) were downstream effectors of the Wnt/β-catenin pathway. A 2013 study found that Wnt/β-catenin signaling is often increased by NOTCH deficiency, as cells may activate alternative pathways to compensate for NOTCH inhibition (Anderson et al., 2013). This resistance mechanism may be responsible for Cyclin D1

and C-myc upregulation in the SK-UT-1B cell line. Like in the SK-LMS-1 cell line, gene expression remained stable in samples treated with a DMSO control.

Ultimately, across both cell lines, MK-0752 was largely more effective than the combination therapy MGD, suggesting that the therapy lacks previously anticipated synergism. Further, gamma-secretase inhibitors were more effective in downregulating downstream effectors of the NOTCH pathway than of the Wnt/β-catenin pathway.

Western Blot

It was hypothesized that C-myc samples treated with the gamma-secretase inhibitor MK-0752 would exhibit lower average intensity and saturation than those treated with the DMSO control. This is visibly reflected in Figure 2, where the MK-0752 treated bands are lighter than those treated with DMSO. Western blot analysis also verified this trend, as the numbers recorded for saturation and intensity post-MK-0752 treatment were lower than those of the control. Such findings support those of previous studies, which found that gamma-secretase inhibitors impair the Wnt/β-catenin pathway, thus resulting in the downregulation of its downstream effectors (Barat et al., 2017). Further, the protein ladder aligned at the point corresponding to 62 kD (C-Myc's molecular weight), confirming the protein's identity as C-Myc and thus further corroborating the above analysis.

Further research is necessary to corroborate and expand upon this study's results. To gather more data points (and hopefully yield more significant results), we plan to retreat all cell lines and perform another round of RNA extraction/qPCR. We also plan to use patient samples to perform immunohistochemistry; this will allow for a more thorough assessment of NOTCH and Wnt/B-catenin behavior and the efficacy of gamma-secretase inhibitors in treating uLMS. Mice models will also be used to assess the effect of MK-0752 on tumor growth. Future studies should further examine MGD and similar gamma-secretase/chemotherapy

combinations to yield clearer and more definitive insights into their synergistic or antagonistic interactions. Lastly, future research should examine the effects of gamma-secretase inhibitors on the uLMS pathway PI3K/AKT/mTOR (PAM) as well as the NOTCH and Wnt/B-Catenin pathways to provide a more comprehensive understanding of their mechanisms.

Acknowledgments:
Thank you to Dr. Douglas for the opportunity to work in her lab; thank you to Dr. Fife, Tracy Wu, Erik Zhou, Trystyn Murphy, and Kaitlyn Heyt for their contributions to this project. Lastly, thank you to Dr. Koppa for providing edits and insight during the writing process.

SCAN FOR BIBLIOGRAPHY

FIELDSTON SCIENCE BULLETIN